Check for updates

Hydrothermally grown novel pyramids of the CaTiO₃ perovskite as an efficient electrode modifier for sensing applications†

Khursheed Ahmad,[a] Praveen Kumar[a] and Shaikh M. Mobin [ID] *[abc]

Herein, we report novel CaTiO₃ pyramids, prepared by a hydrothermal approach using calcium nitrate and titanium butoxide in the presence of sodium hydroxide. The physio-chemical properties of the synthesized CaTiO₃ pyramids were probed by PXRD, FTIR, BET, SEM and EDX. The synthesized CaTiO₃ pyramids possess a good specific surface area which is beneficial for electrochemical applications. Thus, the CaTiO₃ pyramids were applied as an electrode modifier to develop an electrochemical sensor. The working surface area of the glassy carbon (GC) electrode was fabricated with CaTiO₃ pyramids using the drop casting method. This fabricated electrode was employed to determine urea using the cyclic voltammetry and $I-V$ techniques. The fabricated electrode exhibited a good detection limit of 1.6 μM.

1. Introduction

Urea is present in humans and widely distributed in nature. Urea may cause hepatic failure, urinary tract obstruction, nephritic syndrome, cachexia, dehydration, shock and gastrointestinal problems, if its presence (physiological range 1.33–3.33 mM) changes in the blood serum.[1,2] Urea has good solubility in water and is used as a fertilizer. Due to the good solubility of urea in water it may pollute ground and surface water, which can influence human health.[1] Thus, the detection of urea is necessary. In previous years, conventional methods such as chemi-luminescence, electrochemical methods, high performance liquid chromatography, fluorimetry *etc.* have been widely used for the detection of urea.[3,4] However, the electrochemical technique is found to be one of the most promising approaches for the detection of urea due to its low cost, simplicity, high sensitivity and selectivity.[5–7] The performance of electrochemical sensors depends on the nature of the electrode modifiers.[8–10] Parsaee *et al.*[11] employed a NiO-NP/GO modified GCE for urea sensing and a detection limit of 8 μM was obtained. Mikani *et al.*[12] used an F-doped SnO₂ electrode modified with ZnO–Fe₃O₄, whereas Sha *et al.*[13] employed graphene–polyaniline for the determination of urea. Naik *et al.*[14] also introduced a nickel sulfide/graphene oxide modified glassy carbon electrode for urea sensing and achieved a

detection limit of 3.79 μM. Bao *et al.*[15] developed a urea sensor using ultrathin nickel-metal–organic framework nanobelts and the detection limit was found to be 2.23 μM. Hahn and co-workers have grown ZnO nanorods on Ag/glass and used this for the determination of urea.[16] The above observations indicate that electrode modifiers largely influence the performance of the modified electrodes. Therefore, it would be of great importance to design new electrode modifiers.

Recently, perovskite materials with general molecular formula ABO₃ have gained enormous attention because of their excellent optoelectronic applications.[17] Perovskite materials have been used in a variety of applications such as solar cells, batteries, photo-detectors, light emitting diodes, sensors, fuel cells and photocatalysis.[18,19] In 2009, He *et al.*[20] prepared BaTiO₃ perovskite nanocubes for the sensing of hydrogen peroxide. Ahmad *et al.*[21] have synthesized a rGO/SrTiO₃ composite for the determination of nitro-aromatic compounds. In 2020, Shaikh and co-workers employed an N-rGO/SrZrO₃ cuboidal composite for electrochemical determination of hydroquinone.[22] Muthukutty *et al.* also introduced SrSnO₃ as an electrode material for sensing applications.[23] CaTiO₃ has a perovskite structure and possesses good opto-electronic properties and is widely used in photocatalysis.[24] The surface morphology of CaTiO₃ may influence its physiochemical properties. Previously, CaTiO₃ particles were synthesized either by hydrothermal or solvothermal methods. Dong *et al.*[25] have prepared butterfly like dendrites of CaTiO₃, whereas Yang *et al.*[26] have obtained CaTiO₃ hollow micro-cubes. Kimijima *et al.*[24] also synthesized CaTiO₃ cubic particles with controlled size and shape. Wang *et al.*[27] obtained a CaTiO₃ nanolamellate using a hydrothermal approach. It is believed that the design and synthesis of nano-materials with new nanostructures are of

[a] *Discipline of Chemistry, Indian Institute of Technology Indore, Simrol, Khandwa Road, Indore 453552, India. E-mail: xray@iiti.ac.in; Tel: +91-7312438752*

[b] *Discipline of Biosciences and Bio-Medical Engineering, Indian Institute of Technology Indore, Simrol, Khandwa Road, Indore 453552, India*

[c] *Discipline of Metallurgy Engineering and Materials Science, Indian Institute of Technology Indore, Simrol, Khandwa Road, Indore 453552, India*

† Electronic supplementary information (ESI) available. See DOI: 10.1039/d0ma00303d

great importance for the construction of highly efficient electrodes for sensing applications.

Herein, we have synthesized a novel pyramid shaped $CaTiO_3$ perovskite structure using a hydrothermal method and employed it as an electrode material for the electrochemical sensing of urea. To the best of our knowledge, this is the first report on the use of $CaTiO_3$ as electrode materials for urea sensing applications using electrochemical approaches.

2. Materials and methods

2.1. Chemicals and reagents

Calcium nitrate ($Ca(NO_3)_2 \cdot 4H_2O$), titanium(IV) butoxide, phosphate buffered saline solutions, sodium hydroxide (NaOH), polyvinylpyrrolidone, urea, hydrogen peroxide (H_2O_2), ascorbic acid, uric acid, catechol, resorcinol, phenol, dopamine, glucose and other solvents were purchased from Merck, Sigma, SRL, Alfa Aesar and Fischer Scientific, India. All the purchased chemicals/reagents were used without any further purification.

2.2. Synthesis of $CaTiO_3$ pyramids

An aqueous solution (10 mL) of 4 M $Ca(NO_3)_2 \cdot 4H_2O$ (9.446 gm) and 0.4 mL of titanium butoxide ($TiOBu)_4$ were mixed in a round bottom flask slowly, stirred (rpm = ∼900) for 10 min. 6 gm of sodium hydroxide dissolved in deionized water (15 mL) was added dropwise to the reaction mixture and stirred continuously for 30 min. Finally the reaction mixture was transferred to a 50 mL Teflon-lined stainless steel autoclave and heated for 24 h at 180 °C. The white precipitate was collected by centrifugation and washed with 1 M acetic acid and D.I. water several times to remove the unreacted residues.

2.3. Preparation of GC-1 and GC-2 electrodes

The active surface area of a glassy carbon (GC) electrode was cleaned with 0.5 μm alumina slurry and washed with D.I. water. $CaTiO_3$ pyramids were dispersed in D.I. water (1 mg mL^{-1}) using an ultra-sonication bath for 1 h. The active surface area (3 mm = 0.07 cm^2) of the GC was modified with 10 μL of $CaTiO_3$ pyramids. 1 mg of urease was dissolved in 1 mL of PBS

(pH = 7.0) and 10 μL of urease was drop cast on to the $CaTiO_3$ pyramid modified GC electrode to obtain a thin film of urease. Finally 5 μL of 1% polyvinylpyrrolidone (PVP) was also drop cast on to the modified GC (GC/$CaTiO_3$/urease) as a binder. The electrode was kept to dry in air for 4 h. For a controlled experiment, we have modified the GC electrode with urease/PVP. All the modified electrodes were kept in a refrigerator before electrochemical measurements.

3. Results and discussion

3.1. Synthesis of $CaTiO_3$ pyramids

$CaTiO_3$ pyramids were synthesized by mixing calcium nitrate and titanium butoxide in basic medium (NaOH) at 180 °C for 24 h by applying hydrothermal conditions to the reaction mixture (Scheme 1).

3.2. Physiochemical characterization

The powder X-ray diffraction (PXRD) investigation of the synthesized $CaTiO_3$ was carried out using a RINT 2500V X-ray diffractometer (Rigaku, Japan; Cu Kα irradiation; λ = 1.5406 Å). Fig. 1 displays the recorded PXRD pattern of the synthesized $CaTiO_3$ in the 2θ range of 20–80°. The eight major diffraction peaks observed at 23.03°, 32.83°, 38.7°, 40.43°, 47.30°, 59.06°, 69.27° and 78.72° corresponded to the (110), (112), (103), (211), (220), (204), (224) and (116) planes, respectively. The PXRD results were consistent with previously reported literature (JCPDS no. 86-1393).[17,28] The highly intense diffraction peaks suggested the highly crystalline nature of the synthesized $CaTiO_3$. The average crystallite size of the synthesized $CaTiO_3$ was calculated by employing the Debye–Scherrer formula as given in eqn (1) and the average crystallite size of the synthesized $CaTiO_3$ was found to be 96.5 nm.

$$D = \frac{0.9\lambda}{\beta \cos\theta} \qquad (1)$$

(Herein β = the broadening of the diffraction line while λ = 2.2897 Å.)

Further, a Fourier-transform infrared (FTIR) spectroscopic investigation was conducted on a Bio-Rad FTS 300 MX to
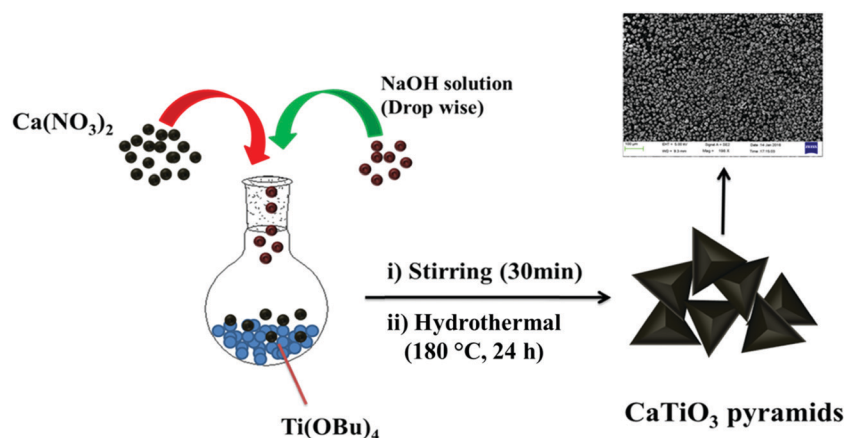
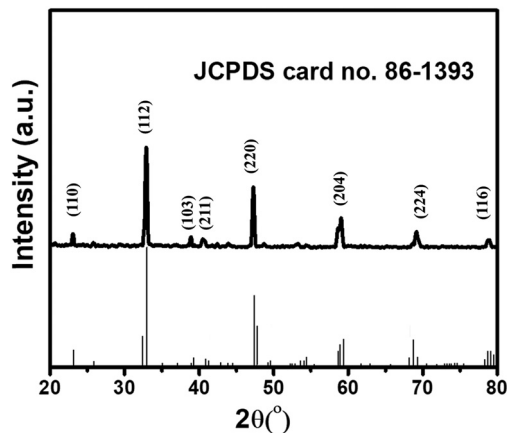**Scheme 1** Schematic representation of the synthesis of $CaTiO_3$ pyramids.

Fig. 1 PXRD pattern of CaTiO₃ pyramids.

understand the presence of chemical bonds in the synthesized CaTiO₃ (Fig. 2). Fig. 2 shows the recorded FTIR spectrum of the synthesized CaTiO₃ in the wavelength range of 4000–400 cm⁻¹. The bands appearing at 3443 and 1639 cm⁻¹ were due to the O–H stretching vibration and deformation of chemisorbed water molecules.[18]

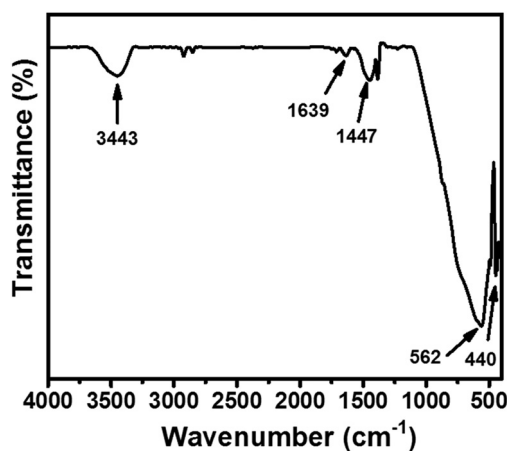**Fig. 2** FTIR of CaTiO₃ pyramids.

The band at 1447 cm⁻¹ is assigned to the CO_3^{2-} bending vibration.[29] The band appearing at 440 cm⁻¹ may be assigned to the stretching vibration of Ti–O, whereas the band at 562 cm⁻¹ may be attributed to bridging stretching of Ti–O–Ti.[18] This also showed the presence of a TiO_6 octahedral environment in the perovskite with ABO_3 structure. The obtained FTIR spectrum was found to be in good agreement with previously reported data.[18,29]

The morphological features of nanomaterials can be affected by the solvent precursor, reaction times, temperature, pH and reactant concentration. It has also been reported that the crystallization mass transport and growth rate of the formation of CaTiO₃ can be governed by the reactant concentration. Previously, CaTiO₃ with butterfly-like dendrites was reported by using water,[25] whereas hollow cubic CaTiO₃ was obtained with polyethylene glycol (PEG) as a solvent.[26] This showed that the solvent largely influences the particle surface morphology. In the present study, CaTiO₃ pyramids were grown using water as a solvent. The particle surface morphology of the synthesized CaTiO₃ was checked on an Oxford Instruments X-max, Aztec (Supra 55 Zeiss Field Emission Scanning Electron Microscope = FE-SEM). The recorded FE-SEM images of CaTiO₃ have been displayed in Fig. 3 and Fig. S1 (ESI†). The FE-SEM results confirmed the pyramid like surface morphology of CaTiO₃. The CaTiO₃ pyramids were grown in a uniform and smooth manner as suggested by the FE-SEM results. To the best of our knowledge, the hydrothermal growth of CaTiO₃ with a pyramid like surface morphology has been achieved for the first time. The exact growth mechanism is not clear but we believe that NaOH may play a significant role in achieving CaTiO₃ pyramids. Nucleation/accumulation was observed at the initial stages (2–4 h) as shown in Fig. S1A and B (ESI†). From 8–18 h, it started to grow in pyramid like structures (Fig. S1C–E, ESI†) and was completely transformed into pyramids of CaTiO₃ after 24 h (Fig. S1F, ESI†).

The presence of the elements in CaTiO₃ was determined on an energy dispersive X-ray (EDX) spectroscope (Oxford Instruments X-max, Aztec). The elemental spectrum and mapping images of Ca, Ti and O have been presented in Fig. 4A–D, respectively. The EDX investigation confirmed the presence of Ca, Ti and O elements in the CaTiO₃ pyramids. Further, the surface area of the synthesized CaTiO₃ was calculated by conducting an N₂ adsorption–desorption
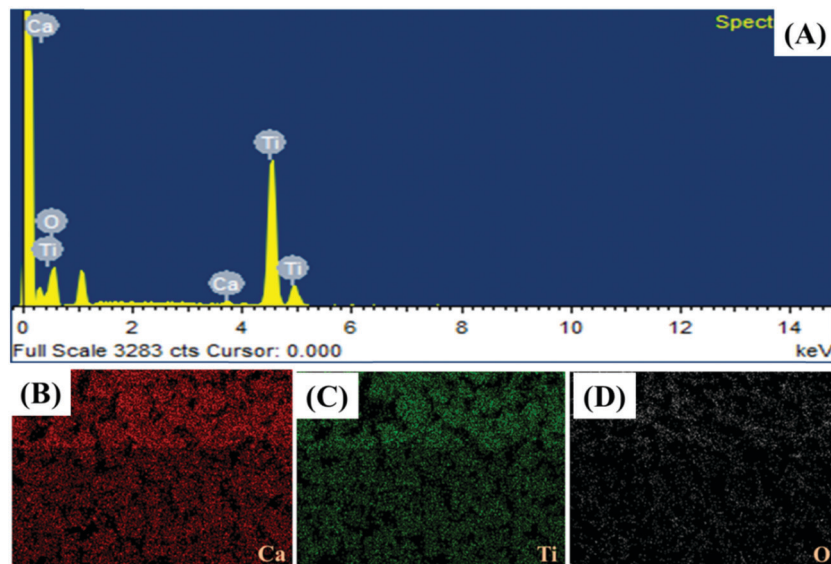

Fig. 3 FE-SEM images of CaTiO₃ pyramids.

| |

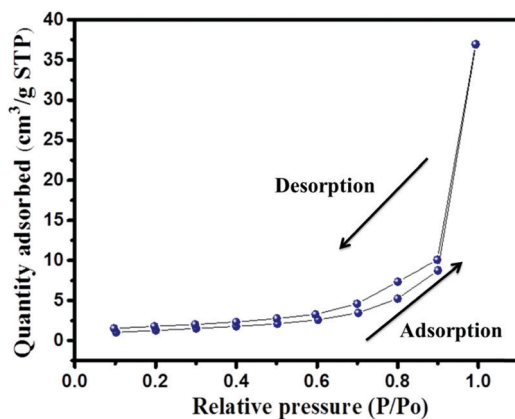**Fig. 4** EDX analysis of CaTiO$_3$ pyramids.

Fig. 5 N$_2$ adsorption–desorption curve of CaTiO$_3$ pyramids.

investigation by using the Brunauer–Emmett–Teller (BET) approach (Autosorb iQ version 1.11; Quantachrome Instruments). The obtained adsorption–desorption curve of the synthesized CaTiO$_3$ has been displayed in Fig. 5.

The specific surface area of the synthesized CaTiO$_3$ was deduced to be 67.5 m^2 g^{-1} (Fig. 5). Hence, it can be proposed that the CaTiO$_3$ perovskite with interesting surface morphology and good surface area may be useful in electrochemical applications. Therefore, we have employed the prepared CaTiO$_3$ pyramids as an electrode modifier for the determination of urea.

3.3. Electrochemical measurements

The electrochemical measurements were carried out on a computer controlled Metrohm Autolab PGSTAT 302N with a three electrode system. The GC electrode was used as the working electrode substrate while platinum wire and Ag/AgCl were used as the counter and reference electrode, respectively. The non-modified GC electrode is denoted as bare GC whereas the GC electrode modified with CaTiO$_3$ pyramids/urease/PVP has been

denoted as **GC-2**. The GC electrode modified with urease/PVP is denoted as **GC-1**.

The charge transfer characteristics of the bare GC and **GC-2** were investigated using electrochemical impedance spectroscopic (EIS) study. The recorded Nyquist plots of the bare GC and **GC-2** were recorded in the presence of 2 mM [Fe(CN)$_6$]$^{3-/4-}$ in 0.1 M PBS (pH = 7.0) with an applied frequency range of 0.01 Hz–100 kHz. Fig. 6 shows the plotted Nyquist plot between the imaginary impedance ($-Z''$) and real impedance (Z'). From Fig. 6, it can be seen that the bare GC has high charge resistance whereas **GC-2** possesses lower charge resistance. It is well understood that high charge resistance limits the electron transport or electron transfer process. This suggested that **GC-2** has good electron transport ability compared to the bare GC due to its low charge resistance.

The cyclic voltammetry (CV) and current–voltage (I–V) approaches were used to probe the electrochemical behavior of **GC-2**. The CV curves of the bare GC and **GC-2** were recorded in the presence of
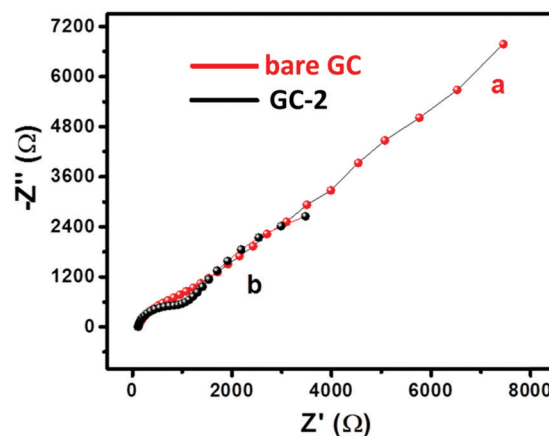

Fig. 6 Nyquist plot of (a) the bare GC and (b) **GC-2** in 2 mM [Fe(CN)$_6$]$^{3-/4-}$ solution in 0.1 M PBS (pH = 7.0).
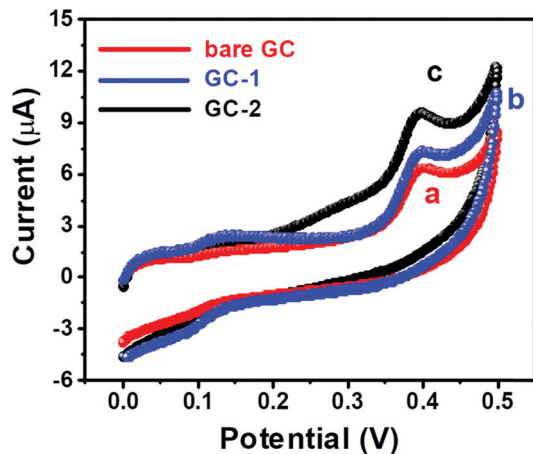
Fig. 7 CV curves of (a) the bare GC, (b) **GC-1** and (c) **GC-2** in the presence of 250 μM urea in 0.1 M PBS (pH = 7.0) at an applied scan rate of 0.1 V s^{-1}.

250 μM urea in 0.1 M PBS (pH = 7.0) with an applied scan rate of 0.1 V s^{-1}. The bare GC showed a current response of 6.3 μA whereas **GC-2** showed 9.8 μA towards the oxidation of 250 μM urea (Fig. 7). This high current response of **GC-2** suggested the successful surface modification of the **GC-2** electrode and better electro-catalytic activity towards the oxidation of urea compared to the bare GC. We have also recorded the CV curve of **GC-1** to check the reason for this enhanced current response of 9.8 μA. **GC-1** exhibited a relatively high current response (7.3 μA) compared to the bare GC, which is due to the presence of catalytic properties in the urease. However, this current response was lower compared to **GC-2**. This showed that the presence of CaTiO$_3$ pyramids with urease significantly enhanced the current response.

Further, I–V curves of the bare GC and **GC-2** were also recorded in the presence of 250 μM urea in 0.1 M PBS (pH = 7.0) with an applied scan rate of 0.1 V s^{-1} (Fig. 8).

The bare GC showed a current response of 8.9 μA, while **GC-2** exhibited a higher current response of 19.51 μA. The obtained results showed a similar trend that **GC-2** has high electro-catalytic ability for the oxidation of urea. Moreover, it was also observed that **GC-2** showed a current response of 8.9 μA
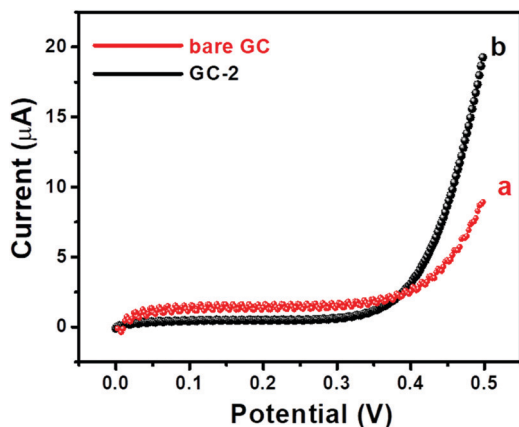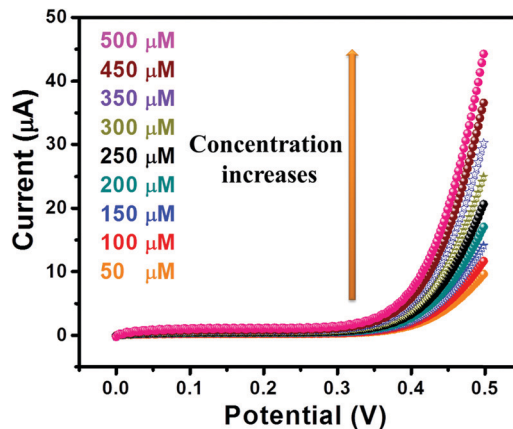

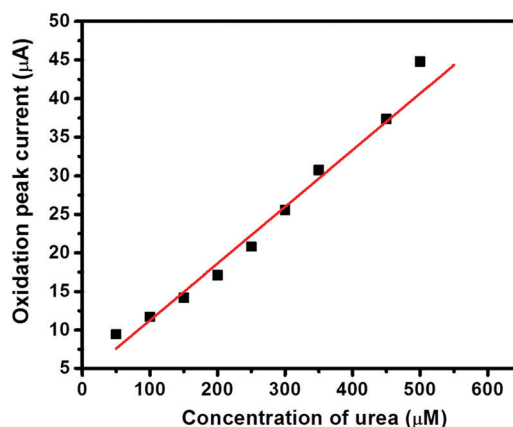Fig. 9 I–V curves of **GC-2** in different concentrations (50–500 μM) of urea in 0.1 M PBS (pH = 7.0).

Fig. 10 Calibration plot of the current peaks against the concentrations of urea.

using CV whereas 19.51 μA was obtained using the I–V technique. Thus, it can be said that the I–V approach is more sensitive in this case. Hence, we have conducted I–V measurements for further electrochemical probes and investigations. The effects of different concentrations of urea on the electrochemical performance of **GC-2** were determined by using the I–V approach.

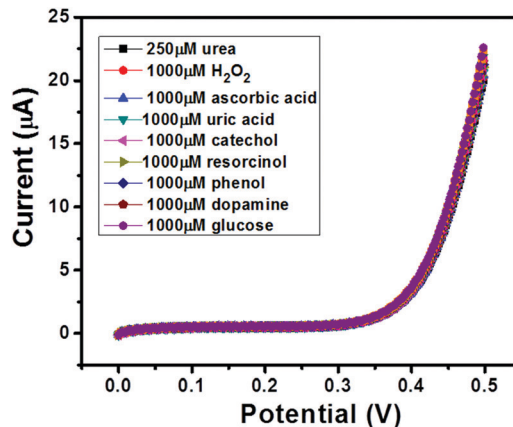
Fig. 8 I–V curves of (a) the bare GC and (b) **GC-2** in the presence of 250 μM urea in 0.1 M PBS (pH = 7.0).

Fig. 11 I–V curves of **GC-2** in the presence of urea (250 μM) in 0.1 M PBS (pH = 7.0) with different interfering species (1000 μM).

The *I–V* curves of **GC-2** in the presence of different concentrations (50–500 μM) of urea in 0.1 M PBS were recorded (Fig. 9). The obtained results showed that the current response was enhanced with increasing the concentration of urea. The linear calibration plot of the current peaks against the concentrations of urea has been presented in Fig. 10. The increase of the current response was found to be linear with respect to the concentration of urea (Fig. 10).

3.4. Selectivity and repeatability studies

The selectivity of a sensor has always been a major concern due to the availability of various electro-active species (such as glucose, uric acid *etc.*) which may affect the electrochemical performance of the sensor in terms of accuracy. Thus, an ideal sensor should be
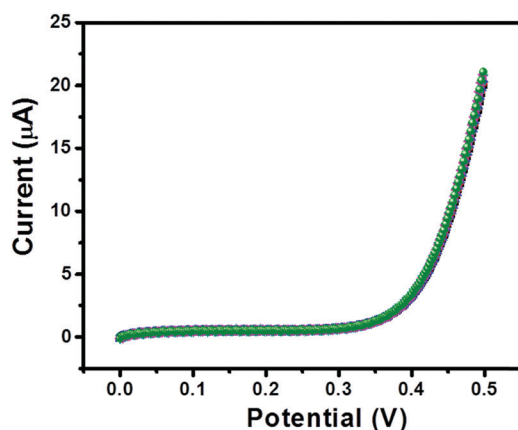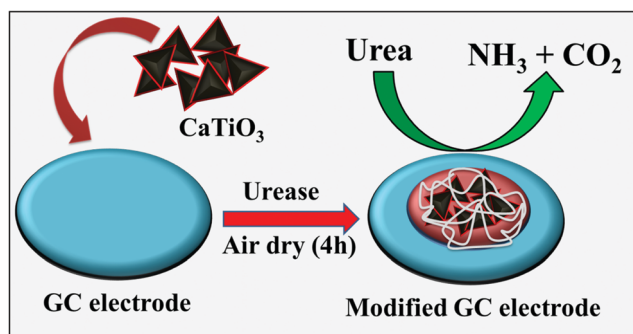

Fig. 12 Five consecutive *I–V* curves of **GC-2** in the presence of urea (250 μM) in 0.1 M PBS (pH = 7.0).

Scheme 2 Schematic illustration of urea sensing.

highly selective. We have performed selectivity studies in the presence of ascorbic acid, hydrogen peroxide, uric acid, catechol, resorcinol, phenol, dopamine and glucose. The *I–V* curves of **GC-2** were recorded in the presence of 250 μM in 0.1 M PBS (pH = 7.0) with interfering species (conc.; 1000 μM) and the obtained results are shown in Fig. 11. There was no significant change in the current response observed even when the concentrations of the electro-active species were 4 times higher than that of urea. Thus, it revealed the good selectivity of **GC-2** towards urea sensing.

Furthermore, the repeatability of the sensor is also an important tool; therefore, we have recorded 5 consecutive *I–V* curves of **GC-2** in the presence of 250 μM urea in 0.1 M PBS (pH = 7.0). The recorded *I–V* curves have been presented in Fig. 12. There was an insignificant change in the current response observed, which indicated its remarkably good repeatability.

The detection limit of the **GC-2** based urea sensor was calculated using the following eqn (2)[21]

$$\text{Detection limit (LOD)} = 3.3 \times \sigma/S \qquad (2)$$

where σ = standard error while S = slope of the calibration curve. The detection limit of the **GC-2** based urea sensor was found to be 1.6 ± 0.2 μM with a linear range of 50–450 μM. The sensitivity was found to be 0.9 μA μM^{-1} cm^{-2} using the formula sensitivity = slope/area of the electrode. The electrochemical oxidation of urea can be represented as shown in Scheme 2. This probable mechanism has been proposed according to previously reported literature.[30–33] The electrochemical oxidation of urea probably produced NH_3 and CO_2 as shown in Scheme 2.

3.5. Comparison

Since the performance of the electrochemical sensor depends on various factors including the nature and quality of the electrode modifiers, hence we have compared the performance of **GC-2** with previously reported literature. Mondal *et al.*[30] employed polypyrrole/Pt as an electrode material for the sensing of urea with a detection limit of 40 μM. Nguyen *et al.*[31] synthesized 3D-graphene/NiCo$_2$O$_4$ and constructed a urea sensor showing a limit of detection of 5 μM. Nguyen *et al.*[32] also constructed a urea sensor based on a NiO/cellulose/CNT electrode modifier which showed a detection limit of 7 μM. Tak *et al.*[33] used a ZnO–MWCNT composite whereas Srivastava *et al.*[34] employed a TiO$_2$–ZrO$_2$ composite for the sensing of urea, but the obtained detection limit was poor. Different electrode modifiers have been developed for urea sensing.[16,35] In particular,

Table 1 Comparison table of the **GC-2** based urea sensor with previously reported sensors

S. no.	Electrode modifier	Detection limit (μM)	Sensitivity (μA mM^{-1} cm^{-2})	Electrode diameter (cm^2)	Ref.
1	Polypyrrole/Pt	40	1.11 μA μM^{-1} cm^{-2}	0.03	30
2	3D-graphene/NiCo$_2$O$_4$	5	166	0.25	31
3	NiO/cellulose/CNT	7	371	0.25	32
4	ZnO–MWCNT composite	230	43.02	0.25	33
5	TiO$_2$–ZrO$_2$ composite	440	2.74	0.25	34
6	(Fc-PAMAM) dendrimers/MWCNTs	50	1.085	—	35
7	ZnO NRs	10	41.64	—	16
8	Vitamin C based NiO	10	—	—	36
9	Ni-MOF/Nafion/GCE	2.23	118.77	—	15
10	NiCo$_2$O$_4$ nanoneedles	1	—	0.03	37
11	**GC-2**	**1.6**	**0.9 μA μM^{-1} cm^{-2}**	**0.07**	**This work**

Arain et al.[36] used vitamin C based NiO as a urea sensor which exhibited a detection limit of 10 μM. Bao et al.[15] used a novel composite of a metal–organic-framework (Ni-MOF/Nafion/GCE) for urea sensing with a good detection limit of 2.23 μM. Amin et al.[37] investigated the electrochemical behavior of $NiCo_2O_4$ nanoneedles towards the sensing of urea and obtained a detection limit of 1 μM. The obtained detection limit in the present work is comparable with the previous reports as shown in Table 1.[15,16,30–37]

4. Conclusion

Pyramid shaped $CaTiO_3$ was synthesized using a hydrothermal method. A glassy carbon electrode was modified by drop casting of $CaTiO_3$ and urease to prepare the working electrode (**GC-2**). This prepared **GC-2** electrode was employed for the determination of urea by employing voltammetric approaches. The developed **GC-2** electrode exhibited a good detection limit and high selectivity towards urea sensing. Moreover, we believe that **GC-2** can also be used in other applications such as fuel cells, supercapacitors or water splitting.

Conflicts of interest

There are no conflicts to declare.

Acknowledgements

References

1 D. Dutta, S. Chandra, A. K. Swain and D. Bahadur, *Anal. Chem.*, 2014, **86**, 5914–5921.

2 M. Tyagi, M. Tomar and V. Gupta, *Biosens. Bioelectron.*, 2013, **41**, 110–115.

3 J. Yoon, D. Lee, E. Lee, Y. S. Yoon and D.-J. Kim, *Electroanal.*, 2019, **31**, 17–21.

4 Y.-L. Liu, R. Liu, Y. Qin, Y. Qin, Q.-F. Qiu, Z. Chen, S.-B. Cheng and W.-H. Huang, *Anal. Chem.*, 2018, **90**, 13081–13087.

5 K. Ahmad, P. Kumar and S. M. Mobin, *Nanoscale Adv.*, 2020, **2**, 502–511.

6 W. Raza and K. Ahmad, *Mater. Lett.*, 2018, **212**, 231–234.

7 K. Ahmad and S. M. Mobin, *Nanoscale Adv.*, 2019, **1**, 719–727.

8 K. Ahmad, P. Kumar and S. M. Mobin, *J. Electrochem. Soc.*, 2019, **166**, B1577–B1584.

9 K. Ahmad and S. M. Mobin, *J. Environ. Chem. Eng.*, 2019, **7**, 103347.

10 K. Ahmad, A. Mohammad and S. M. Mobin, *Electrochim. Acta*, 2017, **252**, 549–557.

11 Z. Parsaee, *Ultrason. Sonochem.*, 2018, **44**, 120–128.

12 M. Mikani, S. Talaei, R. Rahmanian, P. Ahmadi and A. Mahmoudi, *J. Electroanal. Chem.*, 2019, **840**, 285–294.

13 R. Sha, K. Komori and S. Badhulika, *Electrochim. Acta*, 2017, **233**, 44–51.

14 T. S. S. K. Naik, S. Saravanan, K. N. S. Saravana, U. Pratiush and P. C. Ramamurthy, *Mater. Chem. Phys.*, 2020, **245**, 122798.

15 C. Bao, Q. Niu, Z.-A. Chen, X. Cao, H. Wang and W. Lu, *RSC Adv.*, 2019, **9**, 29474–29481.

16 R. Ahmad, N. Tripathy and Y.-B. Hahn, *Sens. Actuators, B*, 2014, **194**, 290–295.

17 S. Som, A. K. Kunti, V. Kumar, V. Kumar, S. Dutta, M. Chowdhury, S. K. Sharma, J. J. Terblans and C. Swart, *J. Appl. Phys.*, 2014, **115**, 193101.

18 Y. Wang, C.-G. Niu, L. Wang, Y. Wang, X.-G. Zhang and G.-M. Zeng, *RSC Adv.*, 2016, **6**, 47873–47882.

19 J. Staniforth, S. E. Evans, O. J. Good, R. J. Darton and R. M. Ormerod, *Dalton Trans.*, 2014, **43**, 15022–15027.

20 X. He, C. Hu, Y. Xi, B. Wan and C. Xia, *Sens. Actuators, B*, 2009, **137**, 62–66.

21 K. Ahmad, A. Mohammad, P. Mathur and S. M. Mobin, *Electrochim. Acta*, 2016, **215**, 435–446.

22 K. Ahmad, P. Kumar and S. M. Mobin, *Nanoscale Adv.*, 2020, **2**, 502–511.

23 B. Muthukutty, R. Karthik, S.-M. Chen and M. Abinaya, *New J. Chem.*, 2019, **43**, 12264–12274.

24 T. Kimijima, K. Kanie, M. Nakaya and A. Muramatsu, *CrystEngComm*, 2014, **16**, 5591–5597.

25 W. Dong, G. Zhao, B. Song, G. Xu, J. Zhou and G. Han, *CrystEngComm*, 2012, **14**, 6990–6997.

26 X. Yang, J. Fu, C. Jin, J. Chen, C. Liang, M. Wu and W. Zhou, *J. Am. Chem. Soc.*, 2010, **132**, 14279–14287.

27 D. Wang, Z. Guo, Y. Chen, J. Hao and W. Liu, *Inorg. Chem.*, 2007, **46**, 7707–7709.

28 G. Dong, X. Xiao, L. Zhang, Z. Ma, X. Bao, M. Peng, Q. Zhang and J. Qiu, *J. Mater. Chem.*, 2011, **21**, 2194–2203.

29 H. K. Yang, J. W. Chung, G. S. R. Raju, B. K. Moon, B. C. Choi, J. H. Jeong and J. H. Kim, *Appl. Surf. Sci.*, 2009, **255**, 5062–5066.

30 S. Mondal and M. V. Sangaranarayanan, *Sens. Actuators, B*, 2013, **177**, 478–486.

31 N. S. Nguyen, G. Das and H. H. Yoon, *Biosens. Bioelectron.*, 2016, **77**, 372–377.

32 N. S. Nguyen and H. H. Yoon, *Sens. Actuators, B*, 2016, **236**, 304–310.

33 M. Tak, V. Gupta and M. Tomar, *J. Mater. Chem. B*, 2013, **1**, 6392–6401.

34 S. Srivastava, A. Ali, P. R. Solanki, P. M. Chavhan, M. K. Pandey, A. Mulchandani, A. Srivastava and B. D. Malhotra, *RSC Adv.*, 2013, **3**, 228–235.

35 D. Esma, D. Muamer, N. N. Jackson and S. Mehmet, *Sens. Actuators, B*, 2017, **246**, 920–926.

36 M. Arain, A. Nafady, Sirajuddin, Z. H. Ibupoto, S. T. H. Sherazi, T. Shaikh, H. Khan, A. Alsalme, A. Niaz and M. Willander, *RSC Adv.*, 2016, **6**, 39001–39006.

37 S. Amin, A. Tahira, A. Solangi, V. Beni, J. R. Morante, X. Liu, M. Falhman, R. Mazzaro, Z. H. Ibupoto and A. Vomiero, *RSC Adv.*, 2019, **9**, 14443–14451.